RESEARCH ARTICLE

WILEY

Peroxisome proliferator-activated receptors signature reveal the head and neck squamous cell carcinoma energy metabolism phenotype and clinical outcome

Yuan Yao¹ | Di Wang² | Yu Zhang³ | Qiaofei Tang² | Zhi Xu² | Lingshan Qin⁴ | Yonggang Qu⁴ | Zhiyong Yan²

Correspondence

Di Wang, Otolaryngology, The Second Affiliated Hospital of Shenyang Medical College, Shenyang, China. Email: wangdi8493@126.com

Abstract

Background: Peroxisome proliferator activating receptors (PPARs) are important regulators of nuclear hormone receptor function, and they play a key role in biological processes such as lipid metabolism, inflammation and cell proliferation. However, their role in head and neck squamous cell carcinoma (HNSC) is unclear.

Methods: We used multiple datasets, including TCGA-HNSC, GSE41613, GSE139324, PRJEB23709 and IMVigor, to perform a comprehensive analysis of PPAR-related genes in HNSC. Single-cell sequencing data were preprocessed using Seurat packets, and intercellular communication was analyzed using CellChat packets. Functional enrichment analysis of PPAR-related genes was performed using Cluster-Profile and GSEA. Prognostic models were constructed using LASSO and Cox regression models, and immunohistochemical analyses were performed using human protein mapping (The Human Protein Atlas).

Results: Our single-cell RNA sequencing analysis revealed distinct cell populations in HNSC, with T cells having the most significant transcriptome differences between tumors and normal tissues. The PPAR features were higher in most cell types in tumor tissues compared with normal tissues. We identified 17 PPAR-associated differentially expressed genes between tumors and normal tissues. A prognostic model based on seven PPAR-associated genes was constructed with high accuracy in predicting 1, 2 and 3 year survival in patients with HNSC. In addition, patients with a low risk score had a higher immune score and a higher proportion of T cells, CD8+ T cells and cytotoxic lymphocytes. They also showed higher immune checkpoint gene expression, suggesting that they might benefit from immunotherapy. PPAR-related genes were found to be closely related to energy metabolism.

Conclusions: Our study provides a comprehensive understanding of the role of PPAR related genes in HNSC. The identified PPAR features and constructed prognostic models may serve as potential biomarkers for HNSC prognosis and treatment response. In addition, our study found that PPAR-related genes can differentiate energy metabolism and distinguish energy metabolic heterogeneity in HNSC, providing new insights into the molecular mechanisms of HNSC progression and therapeutic response.

J Gene Med. 2023;e3605. https://doi.org/10.1002/jgm.3605

¹Department of Interventional Radiology, The People's Hospital of Liaoning Province, Shenyang, China

²Otolaryngology, The Second Affiliated Hospital of Shenyang Medical College, Shenyang, China

³Pharmacy Department, General Hospital of Northern Theater Command, Shenyang, China

⁴China Medical University, Shenyang, China

KEYWORDS

energy metabolism, head and neck squamous cell carcinoma, LASSO regression, PPAR, signature

1 | INTRODUCTION

Head and neck cancer (HNC)¹ is a significant public health concern worldwide, characterized by its high morbidity and mortality rates. This malignancy encompasses a diverse group of tumors that arise in the oral cavity, pharynx, larynx and other anatomical regions of the head and neck. Understanding the epidemiology of HNC is crucial for effective prevention, early detection and treatment strategies. China has witnessed a notable increase in the incidence of HNC over the past few decades. The prevalence of risk factors such as tobacco and alcohol consumption, betel nut chewing and exposure to environmental carcinogens has contributed to the rising burden of HNC in the Chinese population. Additionally, the high prevalence of human papillomavirus^{2,3} (HPV) infection, particularly HPV16, has been implicated in the development of oropharyngeal cancers. Geographically, HNC incidence rates vary across different regions of China, with higher rates observed in areas with a higher prevalence of risk factors. Internationally, HNC exhibits significant geographical variation in its incidence and risk factor profiles. Developed countries, such as the USA, have observed a decline in HNC incidence, primarily attributed to the decreasing prevalence of tobacco smoking. However, the incidence of oropharyngeal cancers associated with HPV infection has been on the rise in several Western countries.

The main treatments for head and neck cancer include surgical resection, radiation therapy and chemotherapy. However, although these treatments can control the progression of the disease to a certain extent, there are still some difficulties and problems. Early diagnosis and screening of head and neck cancers remains a challenge. Because the symptoms of the disease are not obvious, many patients are already in an advanced stage when they are diagnosed, which limits the effectiveness of treatment. Surgical removal is one of the main treatments for head and neck cancer, but surgery can be difficult for some complex tumors. For example, surgical removal of the throat and voice box can lead to loss of speech and swallowing function, negatively affecting the patient's quality of life. In addition, although radiation therapy and chemotherapy can effectively control the growth and spread of tumors, they can also cause a series of side effects. Radiation therapy can cause problems such as dry mouth, difficulty swallowing and skin inflammation, while chemotherapy can trigger adverse reactions such as nausea, vomiting and immunosuppression. The recurrence rate of head and neck cancer is high, and post-treatment monitoring and follow-up is also an important issue. Timely detection and treatment of recurrent lesions is crucial for the survival and prognosis of patients, but there is still a lack of effective monitoring means and follow-up strategies.

Peroxisome proliferator-activated receptors^{4,5} (PPARs) are a group of nuclear receptors that play a crucial role in various physiological processes, including metabolism, inflammation and cell proliferation. Emerging evidence suggests that PPARs also have important implications for cancer progression. PPARs⁶ are classified into three

subtypes: PPAR- α , PPAR- β/δ and PPAR- γ . Each subtype has distinct tissue distribution and functions. PPAR- α is predominantly expressed in the liver, heart and skeletal muscle, and is involved in lipid metabolism. PPAR- β/δ is ubiquitously expressed and regulates fatty acid oxidation and glucose metabolism. PPAR-y is mainly expressed in adipose tissue and plays a key role in adipogenesis and insulin sensitivity. In the context of cancer, PPARs⁷ have been found to exhibit both tumor-promoting and tumor-suppressing effects, depending on the specific cancer type and stage. PPAR-y, in particular, has been extensively studied in various cancers, including breast, colon, prostate and lung cancer. Activation of PPAR-y⁸⁻¹⁰ has been shown to inhibit cancer cell proliferation, induce cell cycle arrest and promote apoptosis. Additionally, PPAR-y activation can also modulate inflammation and angiogenesis, further contributing to its anti-cancer effects. PPAR- α and PPAR- β/δ have been implicated in promoting cancer cell survival and proliferation in certain contexts. For example, PPAR- α activation has been associated with increased tumor growth and metastasis in hepatocellular carcinoma and colorectal cancer.

The PPARs^{7,8} are a class of nuclear receptors that play a pivotal role in regulating lipid and glucose metabolism and maintaining energy homeostasis. There are three subtypes of PPARs: PPAR α , PPAR β/δ , and PPARy, each of which has a distinct expression pattern in different tissues and plays a unique role in energy metabolism. PPARa: Predominantly expressed in the liver, kidney, heart and skeletal muscle, PPAR α is a primary regulator of fatty acid oxidation, involved in the regulation of fatty acid breakdown and energy production. PPAR β/δ is expressed in various tissues throughout the body, including muscle and adipose tissue. PPAR β/δ is considered a key factor in regulating fatty acid oxidation and energy expenditure, and it also plays a role in regulating insulin sensitivity and adipose tissue differentiation. Mainly expressed in adipose tissue, PPARy is a principal factor in regulating adipocyte differentiation and fat storage. PPARy also plays a role in regulating insulin sensitivity and glucose metabolism. The PPARs execute their functions by regulating the expression of a series of genes that encode proteins involved in fatty acid transport, storage and oxidation, as well as proteins involved in glucose metabolism and insulin signaling. Therefore, PPARs play a crucial role in maintaining energy metabolic balance and preventing metabolic diseases such as obesity, type 2 diabetes and cardiovascular diseases.

With the development of computational biology, Wang et al.¹¹ and Yan et al.¹² investigated a variety of prognostic models using weighted correlation network analysis (WGCNA)¹³ as well as public databases.^{14,15} Therefore, the study of PPARs is of great value for the treatment of multiple solid cancers. This study attempts to study the molecular regulatory mechanism related to PPARs by combining computational biology. The prognostic model of PPARs was established to prove their value in the treatment of head and neck cancer and to provide a strong basis for the subsequent research of sequencing level.

2 | METHOD

2.1 | Multi-cohorts and gene set

The Cancer Genome Atlas Program-head and neck squamous cell carcinoma (TCGA-HNSC) dataset consists of genomic data from 504 tumor samples and 44 normal samples of HNSC. This dataset provides a comprehensive view of the genetic alterations and molecular characteristics associated with HNSC, allowing for the identification of potential biomarkers and therapeutic targets.

The GSE41613¹⁶ dataset is a microarray-based dataset comprising 95 samples. It focuses on patients with a specific disease (not specified) and excludes those with a survival time of less than 30 days. This dataset enables the investigation of gene expression patterns and molecular signatures associated with the disease, potentially revealing insights into disease progression and prognosis.

The GSE139324¹⁷ dataset consists of single-cell sequencing data from five tumor samples and five normal samples. This dataset provides a high-resolution view of the cellular heterogeneity within the studied tissue, allowing for the identification of rare cell populations, characterization of cell states, and exploration of tumor microenvironment dynamics.

The PRJEB23709¹⁸ dataset represents a cohort of 71 patients with melanoma who underwent immunotherapy treatment. This dataset includes clinical information, treatment response data and genomic profiles, enabling the investigation of factors influencing response to immunotherapy and the identification of potential predictive biomarkers.

The IMVigor dataset¹⁹ comprises a cohort of 293 patients with bladder cancer who received immunotherapy treatment. This dataset includes clinical data, treatment response information and genomic profiles, providing an opportunity to study the immune landscape of bladder cancer and identify potential biomarkers associated with immunotherapy response. The PPAR gene dataset consists of gene expression data from 69 samples. It focuses on genes involved in the pPAR (PPAR) signaling pathway, which plays a crucial role in regulating various biological processes, including lipid metabolism, inflammation and cell proliferation. This gene set allows for the investigation of PPAR pathway dysregulation in different diseases and the identification of potential therapeutic targets.

2.2 | Single-cell analysis

First, we preprocess the single-cell sequencing data using the Seurat package.²⁰ Seurat provides various functions for quality control, normalization, feature selection and dimensionality reduction of the data. After preprocessing, we use the ggplot2 package to create visualizations of the cell population proportions. This can be done by generating bar plots that represent the proportions of different cell types or clusters identified in the data. To analyze cell-cell communication, we utilize the CellChat package.²¹ CellChat provides methods to identify and characterize intercellular communication networks within single-cell data. It allows you to explore the interactions between different

cell types and identify key signaling pathways. We use the Dorothea²² package. Dorothea provides a comprehensive collection of transcription factor binding site predictions, which can be used to evaluate the activity of specific transcription factors in the single-cell data. This analysis helps in understanding the regulatory mechanisms underlying gene expression patterns. To assess the activity of tumor-related pathways, you can employ the progeny package. Progeny^{23,24} utilizes gene expression data to calculate pathway activity scores, allowing you to evaluate the activation or inhibition of specific pathways in the single-cell data. This analysis provides insights into the functional states of cells within the tumor microenvironment.

2.3 | Functional enrichment analysis of PPAR related genes was performed

ClusterProfile^{25,26} was used for pathway enrichment analysis, which could help us find biological pathways that were significantly enriched in a given gene set, thereby revealing the functional significance of changes in single-cell gene expression. Next, the results of the enrichment analysis were visualized using the gene set enrichment analysis (GSEA)^{27–29} package. GseaVis offers interactive charts and visualization tools to explore enriched gene sets and their relationships in single-cell data.

Finally, RCircos was used to map the chromosomal position. RCircos is an R package for creating circular graphs that visualize genomic data, including the locations of genes on chromosomes. In single-cell analysis, RCircos can be used to visualize the genomic location of a specific gene or set of genes in a circular layout, thereby exploring spatial relationships and genomic organization.

2.4 | HNSC subtypes and prognostic model analysis of PPAR related genes

Least absolute shrinkage and selection operator (LASSO) and Cox regression models were constructed using glmnet. 30 Survminer draws the survival curve, ggplot2, 31,32 and ggpubr draw violin drawings. The timeROC 33,34 package plots the receiver operating characteristic (ROC) curve. Pheatmap draws heat maps and gsva packets calculate channel scores. The immuno-oncology biological research (IOBR) package was evaluated and the proportion of immunoinfiltrated cells was calculated. Survminer draws the survival curve. The ConsensusClusterPlus package was used for consistent cluster analysis.

2.5 | Immunohistochemical analysis and validation analysis

The Human Protein Atlas (HPA) is a comprehensive and publicly available database that provides valuable information on the expression patterns and subcellular localization of proteins in various human tissues and cells. It aims to map the human proteome by systematically profiling the expression of proteins across different tissues and cell

types. The HPA database integrates data from multiple sources, including immunohistochemistry, immunofluorescence and RNA sequencing (RNA-seq), to provide a comprehensive view of protein expression in human tissues. It covers a wide range of tissues, including major organs, such as the brain, heart, liver and kidney, as well as specific cell types, such as immune cells and stem cells. The database provides detailed information on the expression levels of proteins, their subcellular localization and their tissue specificity. It also includes images and annotations that allow users to visualize and interpret the data. Additionally, the HPA database provides access to transcriptomic data, enabling users to explore the correlation between mRNA expression and protein abundance.

2.6 | PPAR-related signature and energy metabolism pathway

The energy metabolism pathways include thiamine metabolism, tryptophan metabolism, tyrosine metabolism, phenylalanine metabolism, sphingolipid metabolism, starch and sucrose metabolism, propanoate metabolism, pyruvate metabolism, retinol metabolism, other glycan degradation, caffeine metabolism, fatty acid degradation, lysine degradation, glutathione metabolism and glycolysis gluconeogenesis. The PPAR genes were analyzed using the energy metabolism pathway with Pearson's correlation coefficient.

3 | RESULTS

3.1 | Single-cell RNA-seq analysis for HNSC

The overall study design is presented in Figure 1. Initially, we down-loaded single-cell RNA-sequencing (scRNA-seq) data from five tumor and five normal tissues from the gene expression omnibus (GEO) database to investigate the characteristics of tumor-infiltrating immune cells. After filtering the single-cell data, we clustered and annotated a total of 20,313 cells from tumor and normal tissues into

five cell types, including natural killer cells, mast cells, myeloid cells, B cells and T cells, as shown in Figures 2A,B and S1. Moreover, the cell type marker genes were specifically expressed in the corresponding cell population, indicating the accuracy of cell annotation, as depicted in Figure 2C,D. The proportion of cells in each patient is illustrated in Figure 2E. Furthermore, we performed differential expression analysis on each cell type between the tumor and normal tissue. The results revealed that the transcriptome features of T cells from tumor and normal tissue were the most different, with 869 differentially expressed genes (DEGs), as shown in Figure 2E. We also conducted transcription factor analysis across various cell types between tumor and normal tissues, as depicted in Figure 3A,B. In addition, we examined the expression correlation between various cell types and the primary tumor pathways between tumor and normal tissues, as illustrated in Figure 3C,D. Analysis of intercellular communication revealed that there were close communication links between cells, and T cells communicated more strongly with other cell populations in the tumor tissue, as shown in Figure 3E.

3.2 | PPAR signature in HNSC single-cell samples

To investigate the role of the PPAR signature in HNSC, we calculated the PPAR signature of each cell and compared the PPAR signature between tumor and normal tissues (Figure 4A,B). As shown in Figure 4C, most cell types from tumor tissues had a higher PPAR signature than those from normal tissues, such as T cells and myeloid cells (Figure 4C). Then, we divided cells into PPAR signature-high and PPAR signature-low based on the median value of PPAR signature score (Figure 4D). Furthermore, 187 up-regulated and 43 down-regulated DEGs were identified in PPAR signature-high cells and DEGs were selected with adjusted *P*-values <0.05 and |logFC| > 0.25 (Figure 4E). GSEA analysis showed that oxidative phosphorylation, MTORC1 signaling, epithelial mesenchymal transformation and G2M checkpoint pathways were significantly up-regulated in PPAR signature-high cells (Figure 4F). The detailed model information can be seen in Table S1.

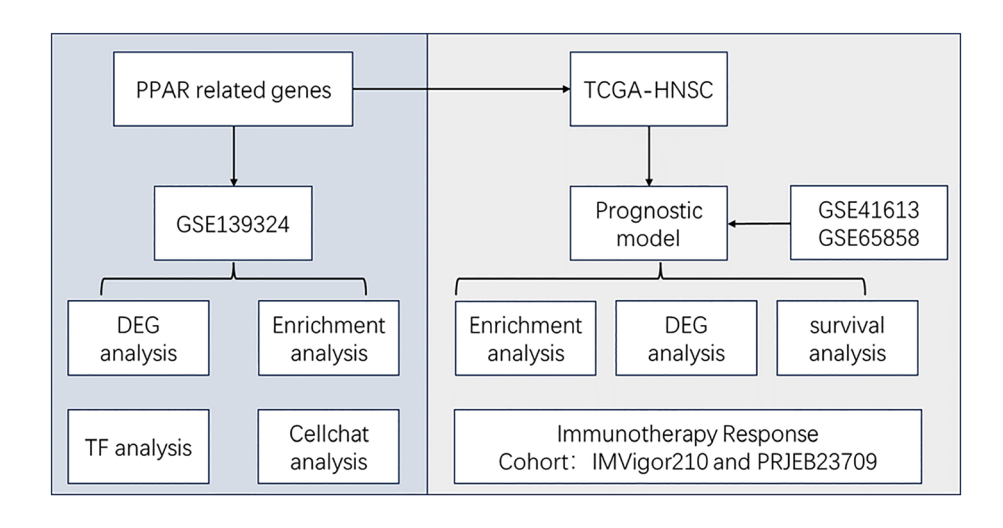


FIGURE 1 The flowchart of the study design.

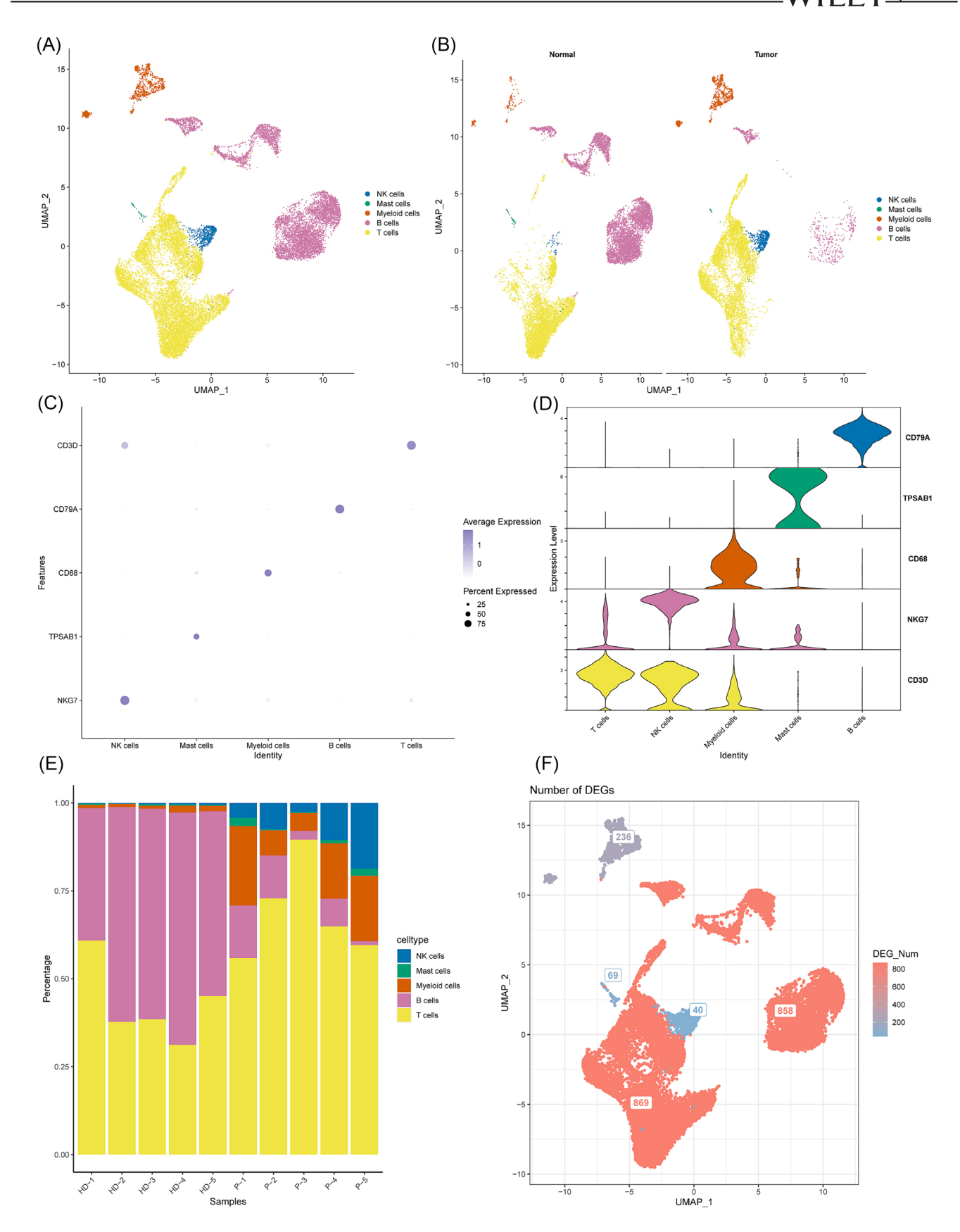


FIGURE 2 Marker gene expression in each cluster. (A) UMAP projection of 20,313 cells from five tumor and normal tissues. (B) UMAP projection of tumor and normal groups. (C) Dot plot showing the expression of marker genes. (D) Violin plot showing the expression of marker genes. (E) Cell type distribution in each sample. (F) UMAP projection of DEGs number in each cell types.

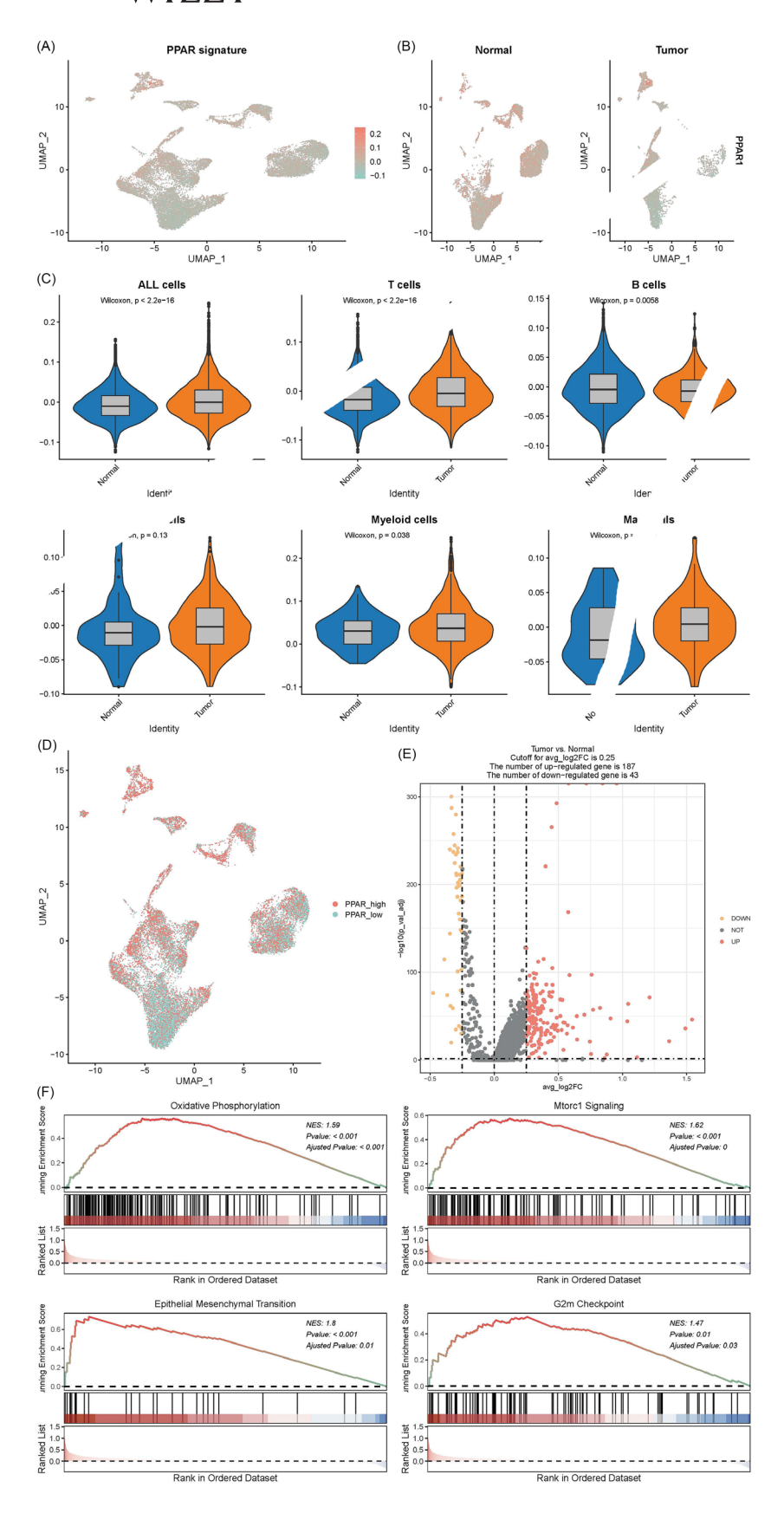


FIGURE 3 Transcription factor, primary tumor pathways, and cell-cell cross talk analysis. (A,B) Heatmap showing the transcription factor (TF) expression in tumor (A) and normal (B) samples among cell types. (C,D) Heatmap showing the primary tumor pathways expression in tumor (C) and normal (D) samples among cell types. (E,F) The results of CellChat analysis.

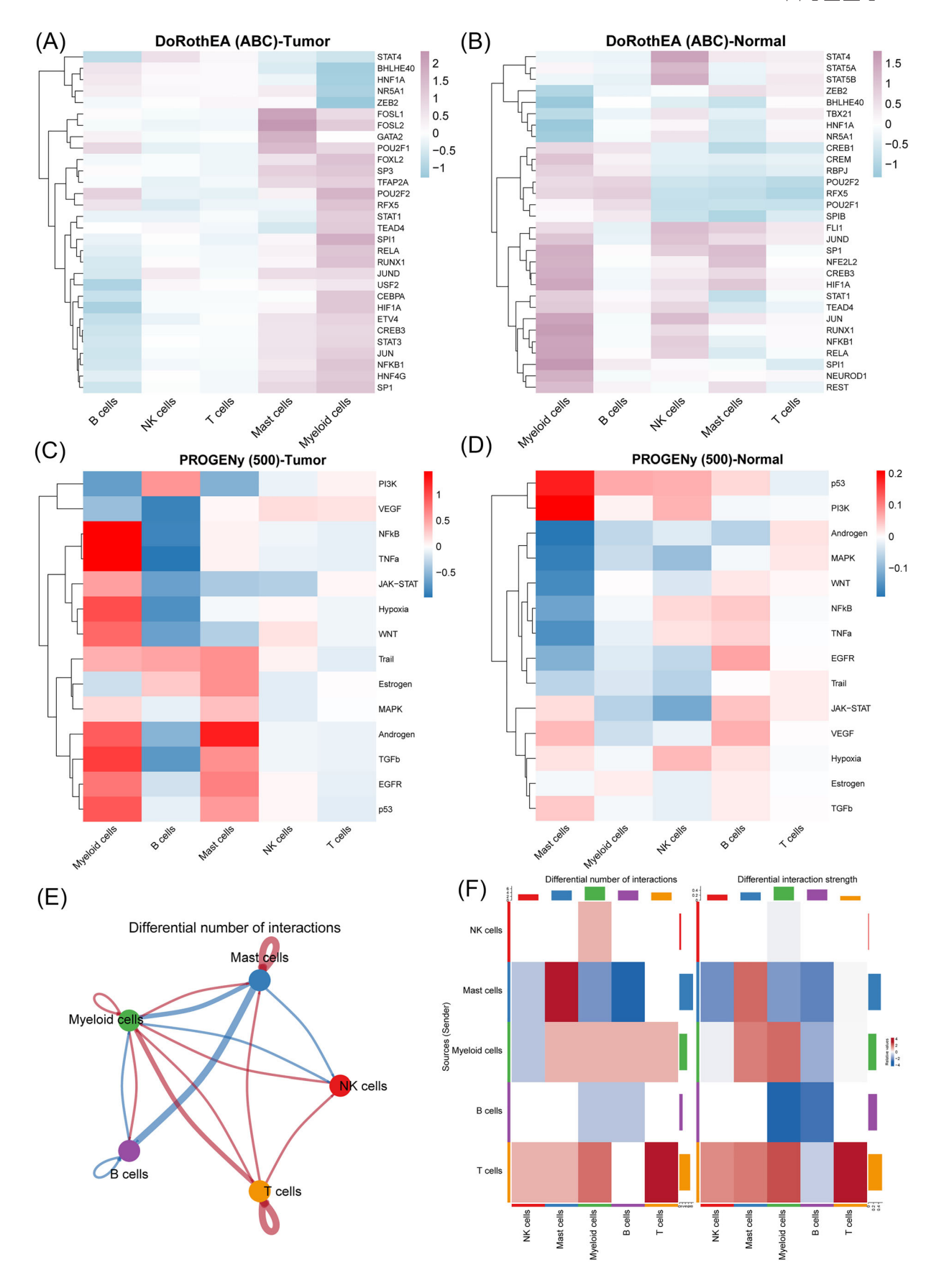


FIGURE 4 Peroxisome proliferator activating receptor (PPAR) signature score between tumor and normal sample. (A) UMAP projection of PPAR signature score. (B) UMAP projection of PPAR signature score in tumor and normal samples. (C) Violin plots showing the PPAR signature score in different cell types between tumor and normal tissue. (D) UMAP projection of cell grouped by PPAR signature. (E) Volcano plot of differentially expressed genes (DEGs) between PPAR-high and low cells. (F) The results of GSEA analysis.

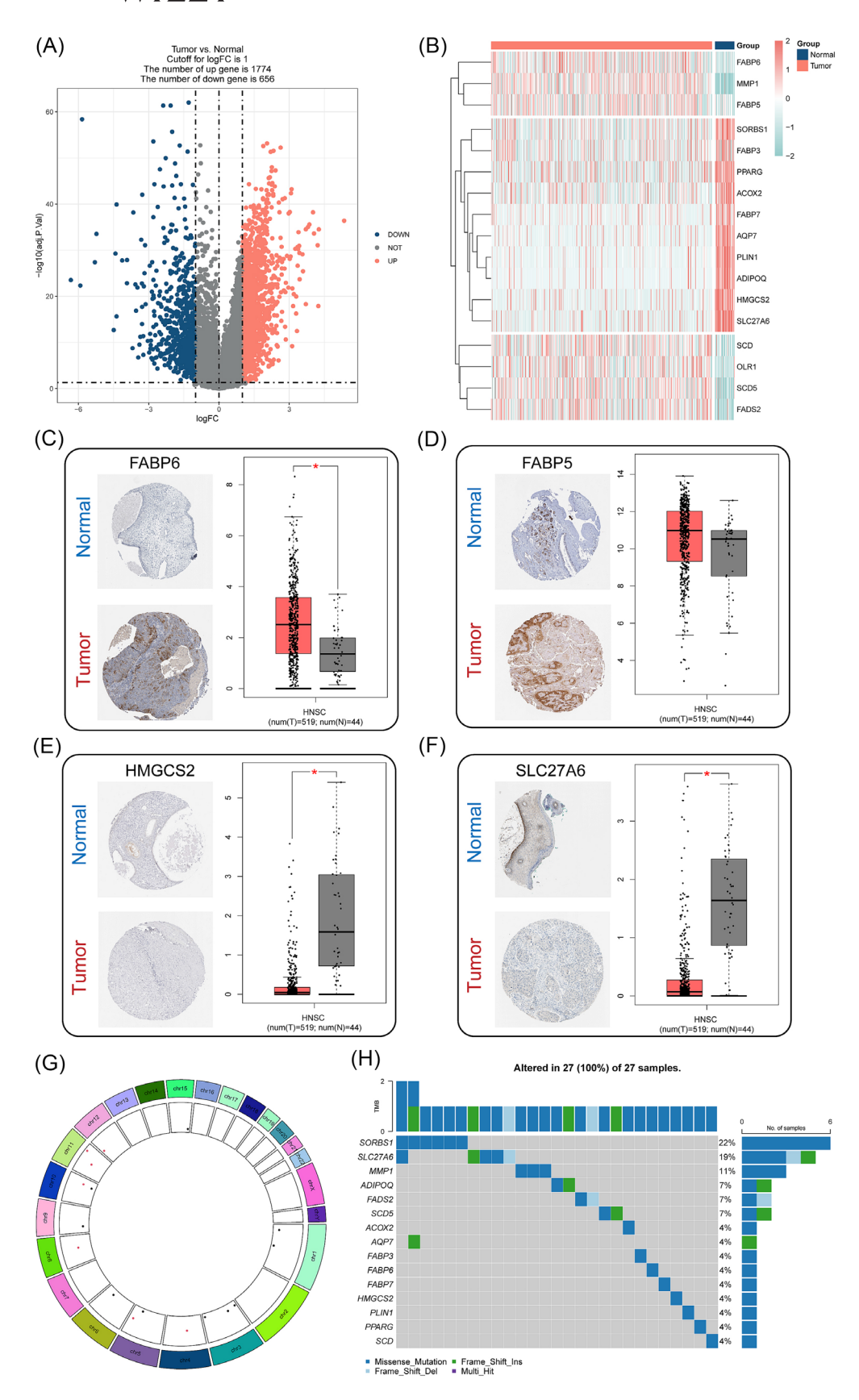


FIGURE 5 Identification of PPAR-related DEGs. (A) Volcano plot of DEGs between tumor and normal sample in TCGA-HNSC. (B) Heatmap showing the differentially expression of 17 PPAR-related DEGs. (C-F) The expression level (protein and mRNA) of FABP6 (C), FABP5 (D), HMGCS2 (E) and SLC27A6 (F) in tumor and normal tissues. (G) The circle plot showing the chromosomal location distribution of 17 PPAR-related DEGs. (H) An oncoplot of PPAR related DEGs.

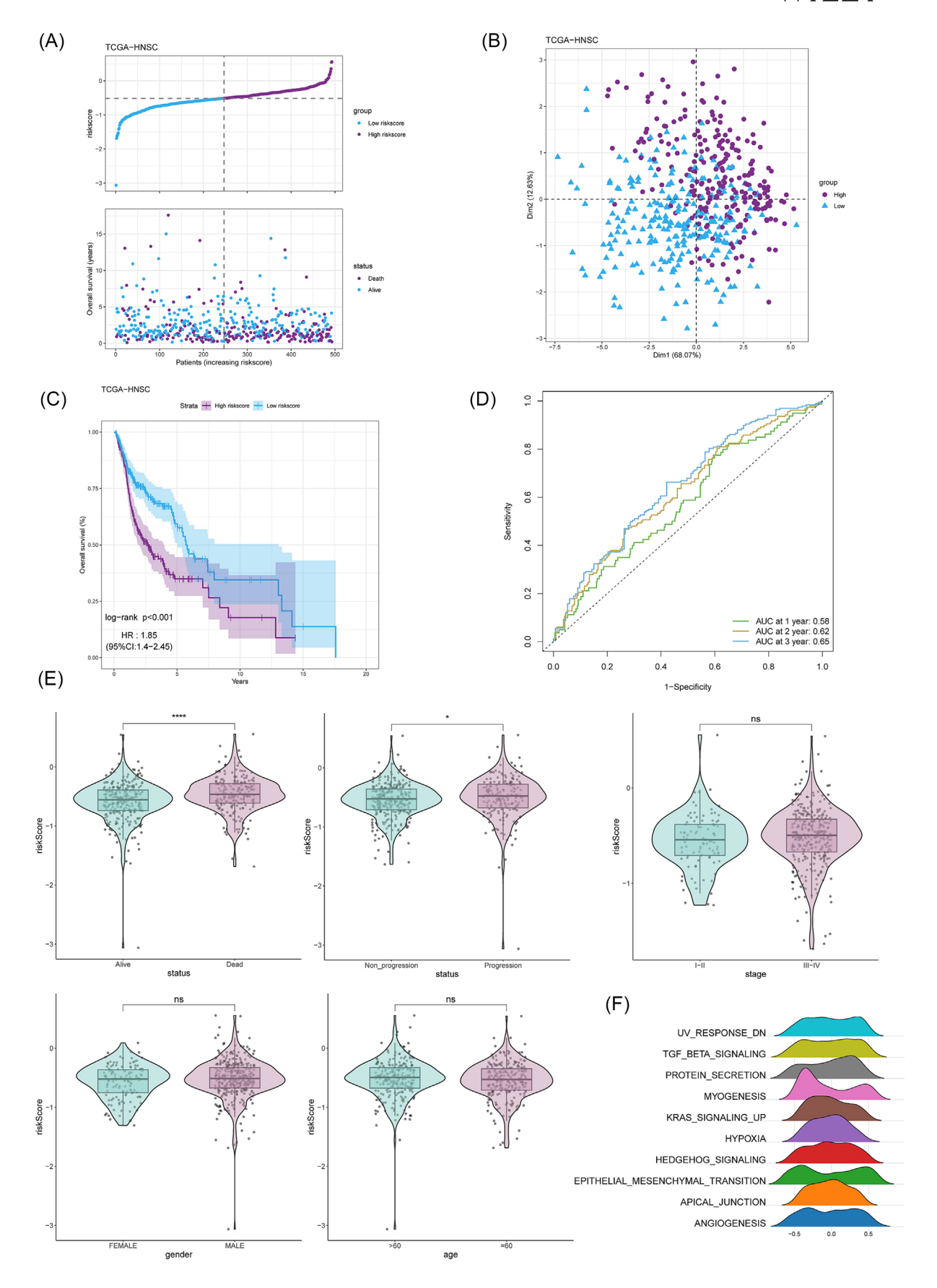


FIGURE 6 Prognostic model development of overall survival (OS) based on PPAR related genes. (A) Distribution of risk score according to the survival status and time in TCGA-HNSC. (B) Principal component analysis plot based on the risk score in TCGA-HNSC. (C) Kaplan-Meier analyses for the high-risk and low-risk groups in TCGA-HNSC cohort. (D) Receiver operating characteristic (ROC) plot based on the risk score in the TCGA-HNSC cohort. (E) The relationship between risk score and clinical features. (F) The ridge plot showing the top 10 pathways based on GSVA analysis.

3.3 | Identification of PPAR-related DEGs

As depicted in Figure 5A, DEG analysis revealed that there were 1774 up-regulated and 656 down-regulated genes in HNSC tissues compared with normal tissues. Additionally, our data indicated that PPARrelated genes exhibited differential expression between tumor and normal tissues. Specifically, up-regulated PPAR-related genes including FABP6, MMP1, FABP5, SCD, OLR1, SCD5 and FADS2 were highly expressed in tumor tissues, while down-regulated PPAR-related genes including SORBS1, FABP3, PPARG, ACOX2, FABP7, AQP7, PLIN1, ADIPOQ, HMGCS2 and SLC27A6 were highly expressed in normal tissues, as shown in Figure 5B. The results based on HPA and GEPIA database analysis showed that at both the protein and mRNA levels, FABP6 and FABP5 exhibited higher expression in tumor samples while both HMGCS2 and SLC27A6 exhibited significantly higher expression in normal samples (Figure 5C-F). The circle diagram in Figure 5G shows the chromosomal locations of the 17 PPAR-related DEGs. Moreover, correlation analysis showed that the expression of each of the 17 PPAR-related DEGs mostly exhibited a positive correlation, as depicted in Figure S2. Notably, the waterfall plot revealed that PPAR-related genes were mutated, with the top three mutated

genes including SORBS1, SLC27A6 and MMP1 having a mutation frequency >10%, as shown in Figure 5H.

3.4 | Prognostic model development and validation of overall survival based on PPAR-related genes

Then we constructed a prognostic model based on seven PPAR related gene according to the LASSO–Cox regression analysis (Figure S3). The following formula was used: risk score $=-0.24334\times ACAA1-0.14841\times ACOX3+0.048727\times ACSL4-0.50133\times ACSL6+0.070616\times MMP1+0.169386*PCK1+0.145317\times PPARG. Afterwards, we calculated the risk scores for each sample in the TCGA-HNSC cohort and divided then into high- and low-risk groups based on the median value of risk score. As shown in Figure 6A, our analysis results showed a higher mortality rate in the high risk patients based on the distributions of risk scores and survival status. Principal component analysis indicated that the classification was satisfactory based on risk score (Figure 6B). Notably, a marked difference was detected in the overall survival (OS) time between$

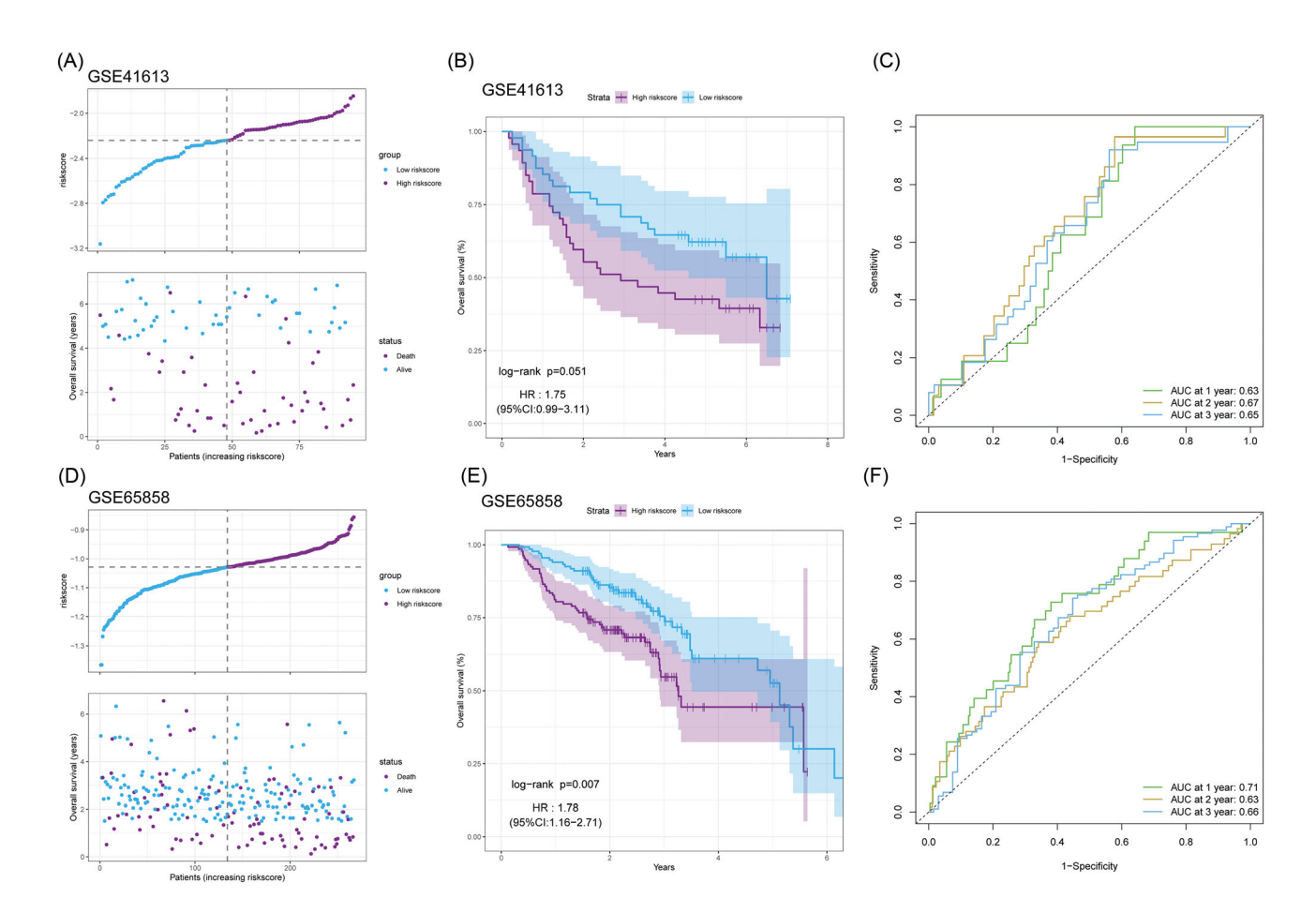


FIGURE 7 Prognostic model validation of OS in GSE41613 and GSE65858 cohort. (A) Distribution of risk score according to the survival status and time in GSE41613 cohort. (B) Kaplan–Meier analyses for the high risk and low risk groups in GSE41613 cohort. (C) ROC plot based on the risk score in the GSE41613 cohort. (D) Distribution of risk score according to the survival status and time in GSE65858 cohort. (E) Kaplan–Meier analyses for the high-risk and low-risk groups in GSE65858 cohort. (F) ROC plot based on the risk score in the GSE65858 cohort.

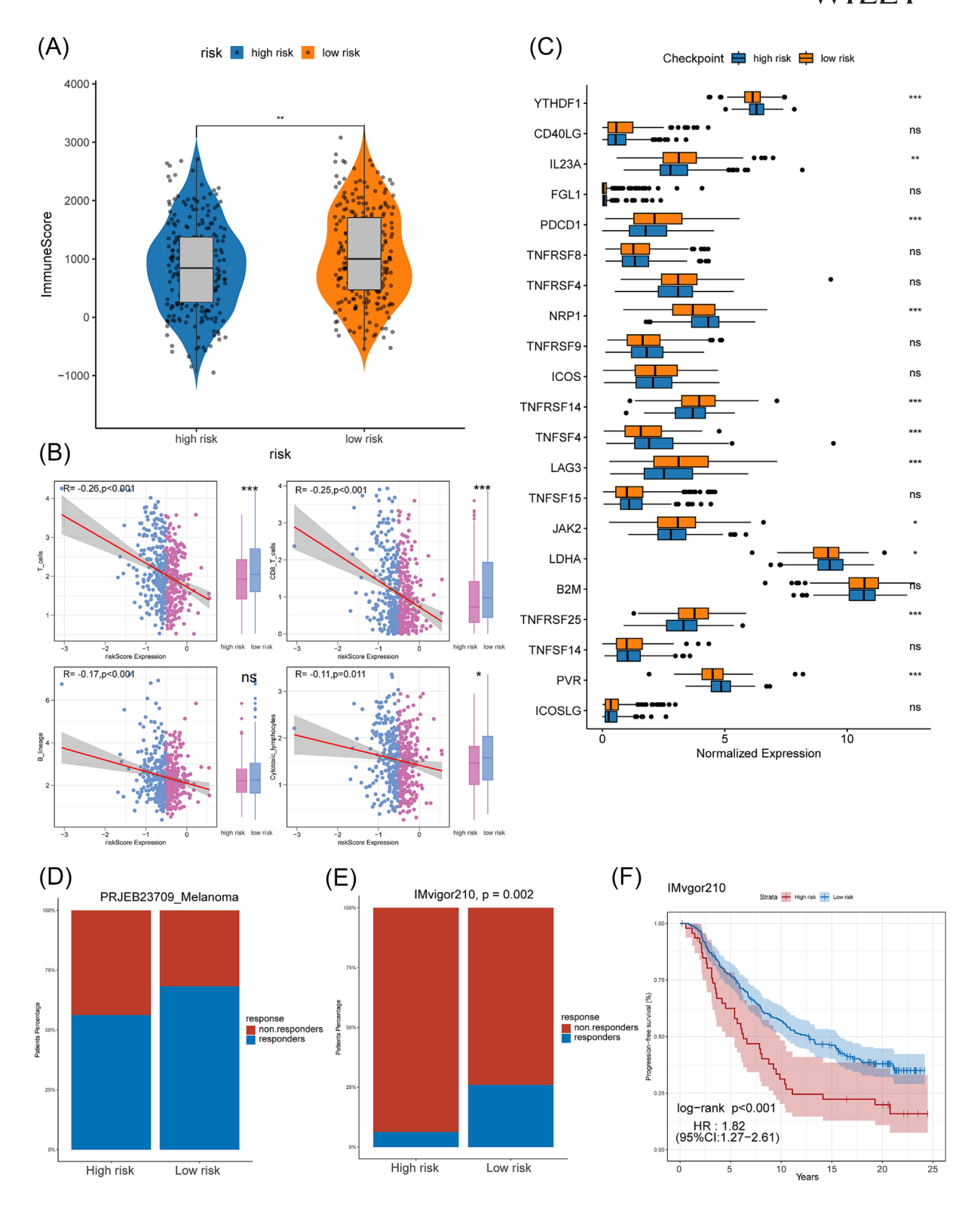


FIGURE 8 Risk score predicted the immunotherapy response. (A) The violin plot showing the immune score for low- and high-risk patients. (B) The relationship between the abundance of T cells, CD8+ T cells, B lineage and cytotoxic lymphocytes and risk score. (C) The boxplot showing the expression of immune checkpoint genes. (D) The barplot showing the distribution of responder and non-responder between high- and low-risk groups in PRJEB23709 cohort. (E) The barplot showing the distribution of responder and non-responder between high- and low-risk groups in IMVigor210 cohort. (F) Kaplan–Meier analyses for the high-risk and low-risk groups in the IMVigor210 cohort.

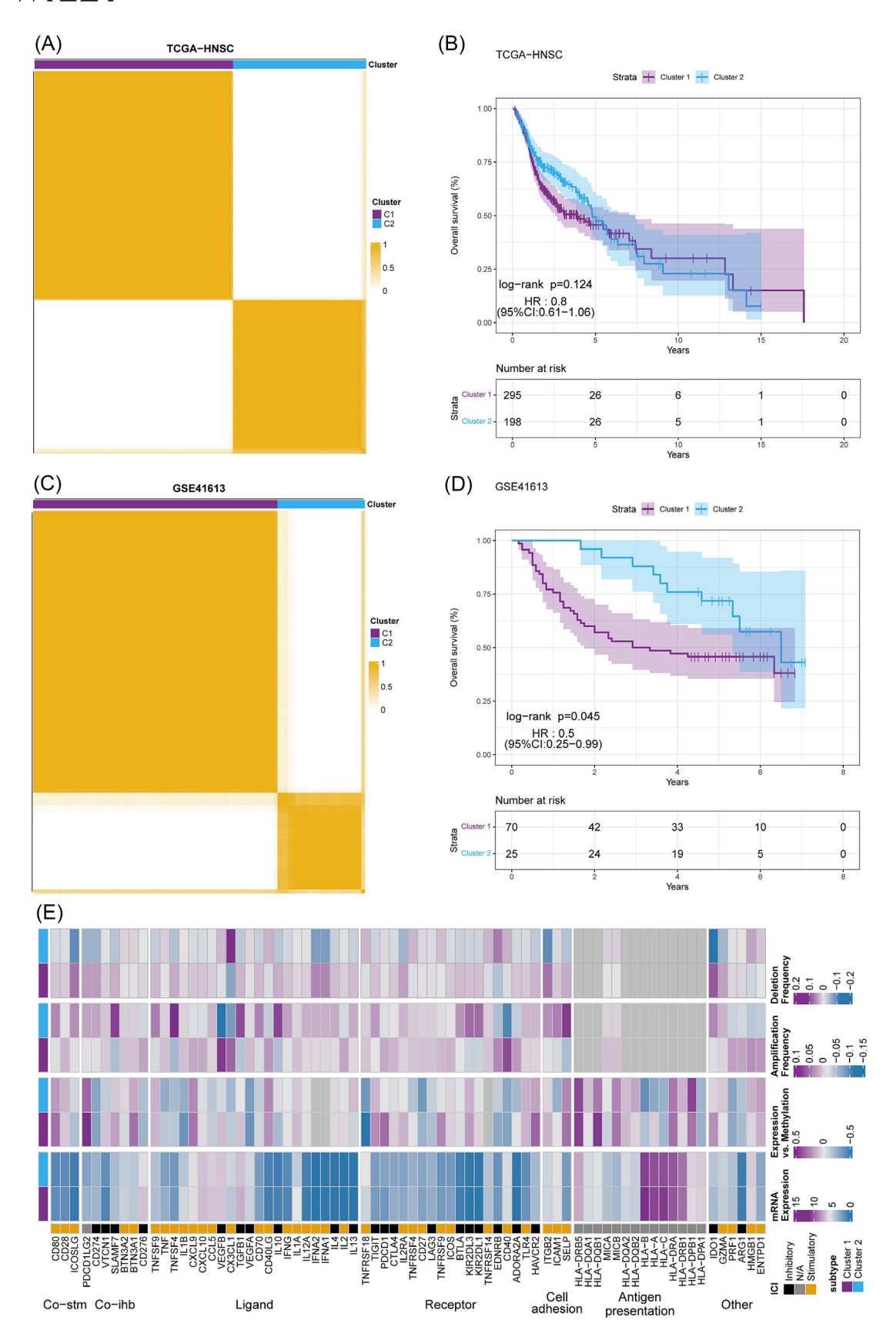


FIGURE 9 Molecular clusters in head and neck squamous cell carcinoma (HNSC). (A) The heatmap showing the HNSC patients were grouped into tow molecular clusters based on seven model gene profiles in the TCGA-HNSC cohort. (B) Kaplan-Meier analyses for the cluster 1 and cluster 2 groups in TCGA-HNSC cohort. (C) The heatmap showing the HNSC patients was grouped into two molecular clusters based on seven model gene profiles in the GSE41613 cohort. (D) Kaplan-Meier analyses for the cluster 1 and cluster 2 groups in the GSE41613 cohort. (E) Heatmap showing mRNA expression; expression vs. methylation; amplification frequency; and the deletion frequency for immune-related genes between cluster 1 and cluster 2 patient.

these two groups and patients with low risk were more likely to have lower death rate (Figure 6C). The ROC curve demonstrated that the prognostic model had high accuracy in predicting 1, 2 and 3 year survival of HNSC patients (Figure 6D). Moreover, risk score was significantly associated with survival status including OS and progression-free survival (PFS), but not age, stage or gender

(Figure 6E). Gene set variation analysis (GSVA) showed the top 10 hall-mark pathways up-regulated in high risk patients, such as hypoxia and kras_signaling_up (Figure 6F). Then, we used two external datasets (GSE41613 and GSE65858) to verify the accuracy of the prognostic model and similar results were obtained, suggesting the prognostic model was reliable and repeated (Figure 7).

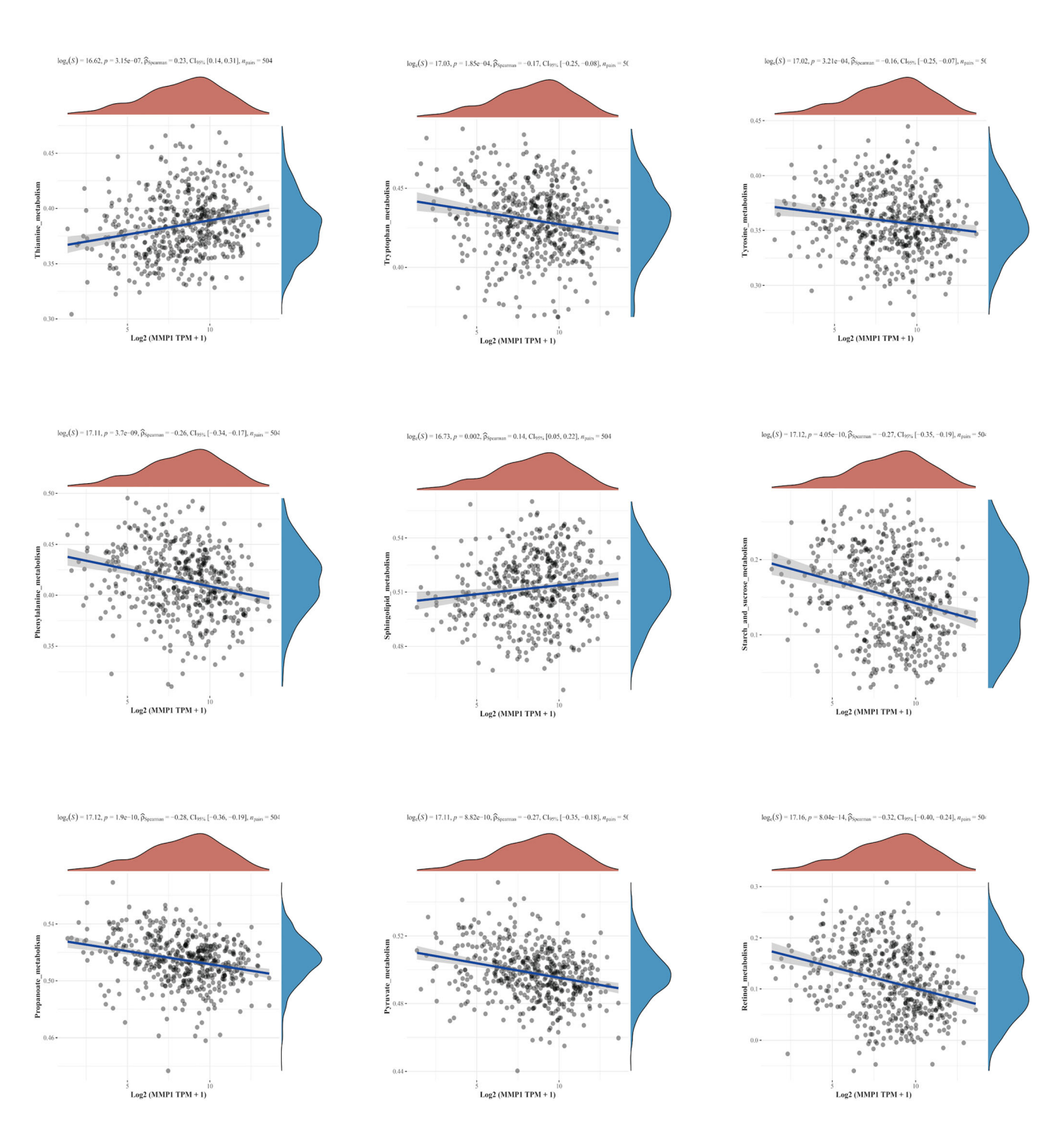


FIGURE 10 MMP1 and energy metabolism Part 1.

3.5 | Risk score predicted immunotherapy response and molecular clusters

To illustrate the relationship between immune characteristics and risk score, we used the "ESTIMATE" R package to calculate the Immune-Score and found that patients with a low risk score had higher levels of ImmuneScore, as shown in Figure 8A. We then examined the abundance of tumor infiltrating immune cells between low- and highrisk-score groups and found that low-risk-score patients had a higher proportion of T cells, CD8+ T cells and cytotoxic lymphocytes, as shown in Figure 8B. We also analyzed the expression of immune checkpoint genes between low- and high-risk-score groups and found that patients with low risk score highly expressed PDCD1, IL23A, TNFRSF14, JAK2 and TNFRSF, suggesting that they may benefit from immunotherapy, as shown in Figure 8C. Our data further showed that a higher proportion of patients in the low-risk group responded to immunotherapy, as shown in Figure 8D,E, and patients with low risk had longer survival time in the immunotherapy cohort, as shown in Figure 8F. Furthermore, using the "ConsensusClusterPlus" R package, we identified two molecular clusters based on seven model genes in HNSC and found that patients in cluster 2 had a survival advantage tendency, as shown in Figure 9A,B. This finding was validated in the GSE41613 dataset, as shown in Figure 9C,D. We observed significant differences in the methylation, amplification and deletion frequency of immunomodulation-related genes between cluster 1 and cluster 2 patients, as shown in the heatmap in Figure 9E. Overall, our findings suggest that risk score can predict immunotherapy response and that molecular clustering based on model genes can identify patients with different survival outcomes.

3.6 | PPAR-related signature and energy metabolism pathway

The thiamine metabolism, tryptophan metabolism, tyrosine metabolism, phenylalanine metabolism, sphingolipid metabolism, starch and sucrose metabolism, propanoate metabolism, pyruvate metabolism, retinol metabolism, other glycan degradation, caffeine metabolism, fatty acid degradation, lysine degradation, glutathione metabolism and glycolysis gluconeogenesis pathways were validated closely in relation to the PPAR-related genes. Therefore, we suggest that the PPAR genes can differentiate energy metabolism and distinguish the heterogeneity of energy metabolism in the head and neck (Figures 10 and 11).

4 | DISCUSSION

This study aimed to investigate the characteristics of tumorinfiltrating immune cells in HNSC using scRNA-seq analysis. The scRNA-seq data from tumor and normal tissues were downloaded from the GEO database and analyzed. Transcription factor analysis and pathway analysis showed distinct patterns of gene regulation and

signaling pathways in different cell types between tumor and normal tissues. Furthermore, the role of the PPAR signature in HNSC was investigated. The PPAR signature was calculated for each cell, and it was found that most cell types in tumor tissues had a higher PPAR signature compared with normal tissues. Differential expression analysis identified up-regulated and down-regulated genes in PPAR signature-high cells. Gene set enrichment analysis revealed the upregulation of pathways related to oxidative phosphorylation, MTORC1 signaling, epithelial-mesenchymal transition and the G2M checkpoint in PPAR signature-high cells. Moreover, PPAR-related genes were found to be differentially expressed between tumor and normal tissues. Up-regulated PPAR-related genes were highly expressed in tumor tissues, while down-regulated PPAR-related genes were highly expressed in normal tissues. The expression of PPARrelated genes showed a positive correlation, and several genes were found to be frequently mutated in HNSC. Based on the PPAR-related genes, a prognostic model for OS was developed using LASSO-Cox regression analysis. The model showed significant differences in OS between high-risk and low-risk groups. The model was validated in an external dataset, demonstrating its reliability. The risk score derived from the model was associated with immune characteristics, immunotherapy response and molecular clusters in HNSC. Therefore, we believe that PPAR-related genes have important research value. Next, we try to further reveal the great significance of PPAR-related genes for targeted therapy of solid tumors by comparing the studies of PPAR in other solid tumors.

Among the five mammalian ACSL family members, ACSL1 and ACSL3 are involved in facilitating cancer progression, while ACSL5 participates in the pro-apoptotic sensing of cells, acting as a tumor suppressor. 35 ACSL4 activates long-chain fatty acids to initiate a number of intracellular lipid metabolic pathway.³⁶ Emerging evidence shows that dysregulated expression of ACSL4 is tightly associated with various diseases, and especially with cancers.³⁷ The mechanisms of ACSL4 involvement in tumor development may include iron-dependent, non-apoptotic and cell death pathways³⁸ Phosphoenolpyruvate carboxykinase 1 (PCK1),³⁹ a key rate-limiting enzyme in gluconeogenesis, catalyzes the conversion of oxaloacetate to phosphoenolpyruvate. The PCK1 expression in gluconeogenic tissues is tightly regulated during fasting. In tumor cells, PCK1 is regulated in a cell-autonomous manner rather than by hormones or nutrients in the extracellular environment. Interestingly, PCK1 has an antioncogenic role in gluconeogenic organs (the liver and kidneys), but a tumor-promoting role in cancers arising from non-gluconeogenic organs. Recent studies have revealed that PCK1 has metabolic and non-metabolic roles in multiple signaling networks linking metabolic and oncogenic pathways. Aberrant PCK1 expression results in the activation of oncogenic pathways, accompanied by metabolic reprogramming, to maintain tumorigenesis. In terms of molecular pathways, we found significant changes in oxidative phosphorylation, MTORC1 signaling, epithelial mesenchymal transformation and G2M checkpoints in different molecular subtypes of the PPAR pathway. Oxidative phosphorylation, MTORC1 signaling, epithelial mesenchymal transformation and G2M checkpoint pathway were significantly

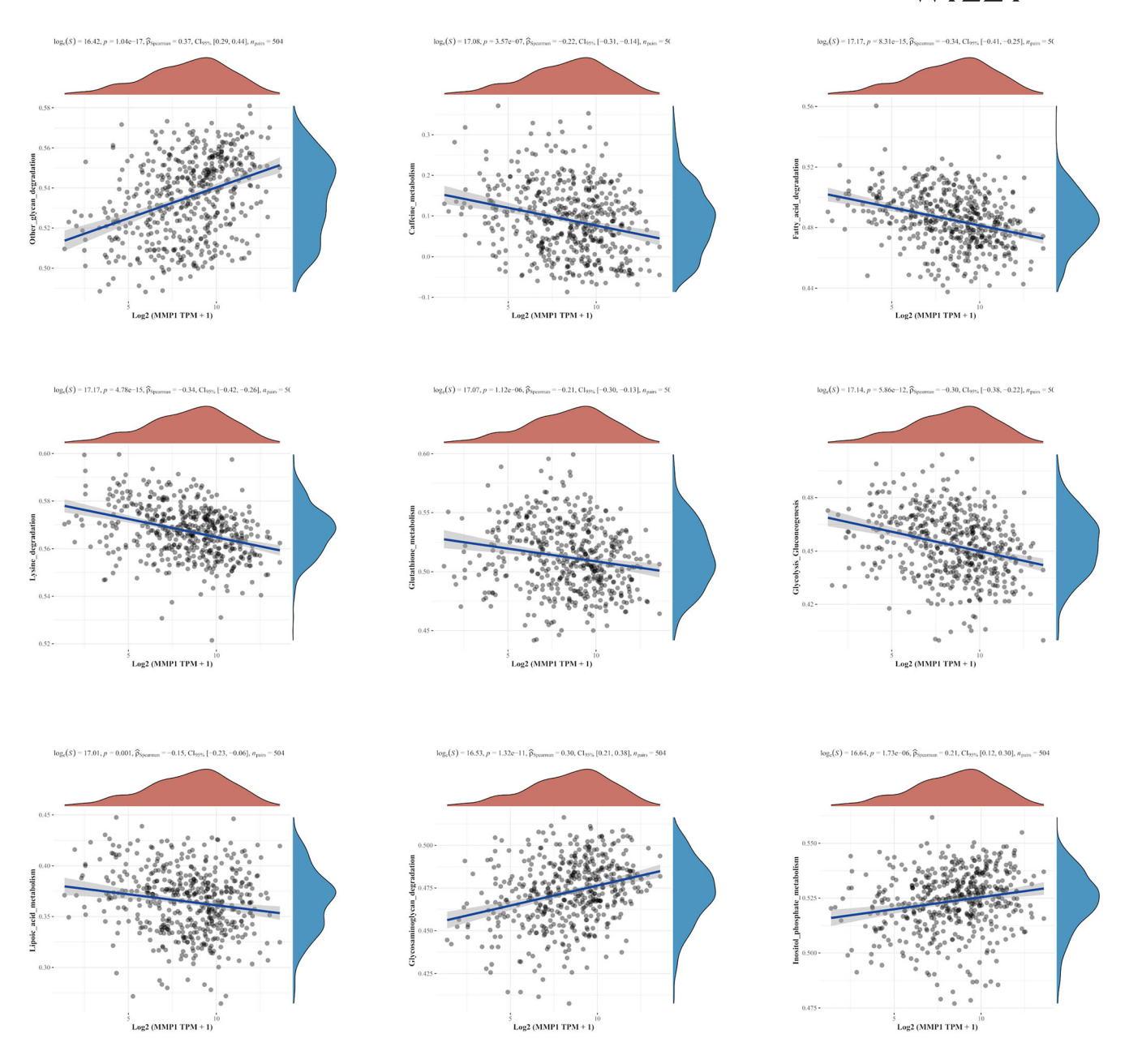


FIGURE 11 MMP1 and energy metabolism Part 2.

upregulated in PPAR cells. Several studies have investigated the crosstalk between PPAR and MTORC1 signaling pathways and their impact on various diseases, including cancer, metabolic disorders and neurodegenerative diseases. These studies have revealed that PPAR activation can modulate MTORC1 activity and downstream signaling pathways, leading to changes in cellular processes such as autophagy, lipid metabolism and inflammation.

Furthermore, emerging evidence suggests that the interaction between PPAR and MTORC1 may have therapeutic implications. For instance, the use of PPAR agonists, such as fibrates and thiazolidinediones, has been explored as a potential strategy to modulate MTORC1 activity and improve the outcomes of various diseases. Recent studies⁴ have shown that PPARs play a significant role in

regulating oxidative phosphorylation. Activation of PPARs has been found to enhance mitochondrial biogenesis, increase the expression of genes involved in oxidative phosphorylation, and improve mitochondrial function. This suggests that PPARs may have a direct impact on the efficiency of ATP production in cells. Furthermore, researchers⁴ have also investigated the crosstalk between PPARs and other signaling pathways involved in oxidative phosphorylation. For example, PPARs have been found to interact with AMP-activated protein kinase, a key regulator of cellular energy metabolism. This interaction can modulate the activity of oxidative phosphorylation enzymes and influence ATP production. Additionally, dysregulation of PPARs and oxidative phosphorylation has been implicated in various metabolic disorders, including obesity, diabetes and cardiovascular

diseases. Understanding the molecular mechanisms underlying the interplay between PPARs and oxidative phosphorylation may provide insights into the development of therapeutic strategies for these conditions. PPAR α regulates lipid metabolism in the liver, the organ that primarily controls nutrient/energy homeostasis throughout the body, abnormalities of which may lead to hepatic steatosis, steatohepatitis, fatty fibrosis and liver cancer. Therefore, we believe that PPAR-related genes may promote the progression of head and neck cancer by affecting the above pathways. However, since this paper is only data-level analysis, further *in vitro* and *in vivo* animal model experiments still need to be verified.

In addition, MMP1 was found to be associated with thiamine metabolism, tryptophan metabolism, tyrosine metabolism, phenylalanine metabolism, sphingolipid metabolism, starch and sucrose metabolism, propanoate metabolism, pyruvate metabolism, retinol metabolism, other glycan degradation, caffeine metabolism and other related pathways. Matrix metalloproteinase-1 (MMP-1) is an enzyme responsible for the degradation of extracellular matrix components such as collagen, elastin and gelatin, especially interstitial collagen types I, II and III. The activity of MMP-1 is strictly regulated at multiple levels, such as gene transcription, preenzyme activation and enzyme inhibition. Dysregulation of MMP-1 metabolism is associated with various pathologic processes such as cancer, fibrosis, arthritis and cardiovascular diseases. For example, in cancer, overexpression of MMP-1 can promote tumor growth, invasion and metastasis by degrading the extracellular matrix and promoting angiogenesis. Conversely, inhibiting the activity of MMP-1 has been explored as a strategy for cancer treatment. In fibrotic diseases, MMP-1 can promote tissue remodeling and fibrosis by degrading collagen and other extracellular matrix components. Therefore, regulating the activity of MMP-1 is considered a potential treatment for these diseases. Overall, MMP-1 plays a key role in the metabolism of the extracellular matrix, and dysregulation of its metabolism can lead to various pathological conditions. Further studies are needed to fully understand the mechanisms of MMP-1 metabolism and to develop effective therapeutic strategies against MMP-1.

In addition, the research has some other limitations. The research involves multiple cancer types and different sample sources, and there is considerable heterogeneity between the data. This makes crosscancer comparisons and analyses difficult and additional data standardization and correction may be required. The samples in this research are mainly from cancer patients, and there is a lack of control samples from healthy people. This makes it difficult to identify which genetic variants are associated with cancer rather than normal physiological changes. The research focused primarily on cancer patients in the USA and lacked samples from other regions and ethnicities. This may limit the generalizability of the findings, as different ethnic and geographical backgrounds may have different cancer pathogenesis and genetic variations. Although the data from the research has been publicly released, owing to the complexity and scale of the data, there are still certain thresholds for non-expert researchers to access and analyze the data. This may limit the utilization and discovery of the data by the broader scientific community.

In conclusion, this study provides insights into the characteristics of energy metabolism the role of PPAR-related genes in HNSC. The developed prognostic model based on PPAR-related genes shows promise in predicting patient outcomes and immunotherapy response. These findings contribute to a better understanding of HNSC and may guide future therapeutic interventions.

ACKNOWLEDGEMENTS

Thanks to Beijing Biology (Xinshi) and NGS assistant for copy editing.

CONFLICT OF INTEREST STATEMENT

Not applicable.

DATA AVAILABILITY STATEMENT

The data can be obtained by the corresponding author.

REFERENCES

- Zhang C, Dang D, Wang H, Shi S, Dai J, Yang M. Acircadian rhythmrelated gene signature for predicting survival and drug response in HNSC. Front Immunol. 2022;13:1029676. doi:10.3389/fimmu.2022. 1029676
- Piña-Sánchez P. Human papillomavirus: challenges and opportunities for the control of cervical cancer. Arch Med Res. 2022;53(8):753-769. doi:10.1016/j.arcmed.2022.11.009
- Zou K, Huang Y, Li Z. Prevention and treatment of human papillomavirus in men benefits both men and women. Front Cell Infect Microbiol. 2022;12:1077651. doi:10.3389/fcimb.2022.1077651
- Christofides A, Konstantinidou E, Jani C, Boussiotis VA. The role of peroxisome proliferator-activated receptors (PPAR) in immune responses. *Metabolism*. 2021;114:154338. doi:10.1016/j.metabol. 2020.154338
- Han X, Wu Y, Yang Q, Cao G. Peroxisome proliferator-activated receptors in the pathogenesis and therapies of liver fibrosis. *Pharma-col Ther.* 2021;222:107791. doi:10.1016/j.pharmthera.2020.107791
- Psilopatis I, Vrettou K, Fleckenstein FN, Theocharis S. The role of peroxisome proliferator-activated receptors in preeclampsia. *Cell.* 2023; 12(4):647. doi:10.3390/cells12040647
- Psilopatis I, Vrettou K, Troungos C, Theocharis S. The role of peroxisome proliferator-activated receptors in endometrial cancer. *Int J Mol Sci.* 2023;24(11):9190. doi:10.3390/ijms24119190
- Escandon P, Vasini B, Whelchel AE, et al. The role of peroxisome proliferator-activated receptors in healthy and diseased eyes. Exp Eye Res. 2021;208:108617. doi:10.1016/j.exer.2021.108617
- Fougerat A, Montagner A, Loiseau N, Guillou H, Wahli W. Peroxisome proliferator-activated receptors and their novel ligands as candidates for the treatment of non-alcoholic fatty liver disease. *Cell.* 2020;9(7): 1638. doi:10.3390/cells9071638
- Abushouk AI, El-Husseny M, Bahbah EI, et al. Peroxisome proliferator-activated receptors as therapeutic targets for heart failure. *Biomed Pharmacother*. 2017;95:692-700. doi:10.1016/j.biopha. 2017.08.083
- 11. Wang Y, Yan K, Lin J, et al. CD8+ T cell co-expressed genes correlate with clinical phenotype and microenvironments of urothelial cancer. *Front Oncol.* 2020;10:553399. doi:10.3389/fonc.2020.553399
- 12. Yan K, Lu Y, Yan Z, Wang Y. 9-gene signature correlated with CD8(+) T cell infiltration activated by IFN-γ: a biomarker of immune checkpoint therapy response in melanoma. *Front Immunol.* 2021;12: 622563. doi:10.3389/fimmu.2021.622563
- Hu D, Cao Q, Tong M, et al. A novel defined risk signature based on pyroptosis-related genes can predict the prognosis of prostate cancer.

- BMC Med Genomics. 2022;15(1):24. doi:10.1186/s12920-022-01172-5
- Wang Y, Yan K, Wang J, Lin J, Bi J. M2 macrophage co-expression factors correlate with immune phenotype and predict prognosis of bladder cancer. Front Oncol. 2021;11:609334. doi:10.3389/fonc. 2021.609334
- Wang Y, Yan K, Lin J, et al. Three-gene risk model in papillary renal cell carcinoma: a robust likelihood-based survival analysis. Aging (Albany NY). 2020;12(21):21854-21873. doi:10.18632/aging.104001
- Wang Y, Nakajima T, Gonzalez FJ, Tanaka N. PPARs as metabolic regulators in the liver: lessons from liver-specific PPAR-null mice. Int J Mol Sci. 2020;21(6):2061. doi:10.3390/ijms21062061
- Ruffin AT, Cillo AR, Tabib T, et al. B cell signatures and tertiary lymphoid structures contribute to outcome in head and neck squamous cell carcinoma. *Nat Commun.* 2021;12(1):3349. doi:10.1038/s41467-021-23355-x
- Gide TN, Quek C, Menzies AM, et al. Distinct immune cell populations define response to anti-PD-1 monotherapy and anti-PD-1/anti-CTLA-4 combined therapy. Cancer Cell. 2019;35(2):238-255. e6. doi:10.1016/j.ccell.2019.01.003
- Massari F, Di Nunno V, Cubelli M, et al. Immune checkpoint inhibitors for metastatic bladder cancer. Cancer Treat Rev. 2018;64:11-20. doi: 10.1016/j.ctrv.2017.12.007
- Zhao X, Wu S, Fang N, Sun X, Fan J. Evaluation of single-cell classifiers for single-cell RNA sequencing data sets. *Brief Bioinform*. 2020; 21(5):1581-1595. doi:10.1093/bib/bbz096
- Jin S, Guerrero-Juarez CF, Zhang L, et al. Inference and analysis of cell-cell communication using CellChat. *Nat Commun*. 2021;12(1): 1088. doi:10.1038/s41467-021-21246-9
- Li G, Peng L, Wu M, Zhao Y, Cheng Z, Li G. Appropriate level of cuproptosis may be involved in alleviating pulmonary fibrosis. Front Immunol. 2022;13:1039510. doi:10.3389/fimmu.2022.1039510
- Giordani L, He GJ, Negroni E, et al. High-dimensional single-cell cartography reveals novel skeletal muscle-resident cell populations. *Mol Cell*. 2019;74(3):609-621.e6. doi:10.1016/j.molcel.2019.02.026
- 24. Tirosh I, Venteicher AS, Hebert C, et al. Single-cell RNA-seq supports a developmental hierarchy in human oligodendroglioma. *Nature*. 2016;539(7628):309-313. doi:10.1038/nature20123
- Yu G, Wang LG, Han Y, He QY. clusterProfiler: an R package for comparing biological themes among gene clusters. *Omics*. 2012;16(5): 284-287. doi:10.1089/omi.2011.0118
- Wu T, Hu E, Xu S, et al. clusterProfiler 4.0: a universal enrichment tool for interpreting omics data. *Innovation (Camb)*. 2021;2(3):100141. doi:10.1016/j.xinn.2021.100141
- Powers RK, Goodspeed A, Pielke-Lombardo H, Tan AC, Costello JC. GSEA-InContext: identifying novel and common patterns in expression experiments. *Bioinformatics*. 2018;34(13):i555-i564. doi:10.1093/bioinformatics/bty271
- 28. Eraso-Pichot A, Brasó-Vives M, Golbano A, et al. GSEA of mouse and human mitochondriomes reveals fatty acid oxidation in astrocytes. *Glia*. 2018;66(8):1724-1735. doi:10.1002/glia.23330
- Subramanian A, Tamayo P, Mootha VK, et al. Gene set enrichment analysis: a knowledge-based approach for interpreting genome-wide

- expression profiles. *Proc Natl Acad Sci U S A*. 2005;102(43):15545-15550. doi:10.1073/pnas.0506580102
- Dalal SR, Shekelle PG, Hempel S, Newberry SJ, Motala A, Shetty KD.
 A pilot study using machine learning and domain knowledge to facilitate comparative effectiveness review updating. *Med Decis Making*. 2012;33(3):343-355. doi:10.1177/0272989X12457243
- Wu X, Sui Z, Zhang H, Wang Y, Yu Z. Integrated analysis of IncRNAmediated ceRNA network in lung adenocarcinoma. Front Oncol. 2020; 10:554759. doi:10.3389/fonc.2020.554759
- Ito K, Murphy D. Application of ggplot2 to pharmacometric graphics. CPT Pharmacometrics Syst Pharmacol. 2013;2(10):e79. doi:10.1038/psp.2013.56
- 33. Song M, Zhang Q, Song C, et al. The advanced lung cancer inflammation index is the optimal inflammatory biomarker of overall survival in patients with lung cancer. *J Cachexia Sarcopenia Muscle*. 2022;13(5): 2504-2514. doi:10.1002/jcsm.13032
- Xu Y, Wang X, Huang Y, Ye D, Chi P. A LASSO-based survival prediction model for patients with synchronous colorectal carcinomas based on SEER. *Transl Cancer Res.* 2022;11(8):2795-2809. doi:10.21037/tcr-20-1860
- 35. Quan J, Bode AM, Luo X. ACSL family: the regulatory mechanisms and therapeutic implications in cancer. *Eur J Pharmacol*. 2021;909: 174397. doi:10.1016/j.ejphar.2021.174397
- Kuwata H, Hara S. Role of acyl-CoA synthetase ACSL4 in arachidonic acid metabolism. *Prostaglandins Other Lipid Mediat*. 2019;144: 106363. doi:10.1016/j.prostaglandins.2019.106363
- Dattilo MA, Benzo Y, Herrera LM, et al. Regulatory mechanisms leading to differential acyl-CoA synthetase 4 expression in breast cancer cells. Sci Rep. 2019;9(1):10324. doi:10.1038/s41598-019-46776-7
- 38. Doll S, Proneth B, Tyurina YY, et al. ACSL4 dictates ferroptosis sensitivity by shaping cellular lipid composition. *Nat Chem Biol.* 2017;13(1): 91-98. doi:10.1038/nchembio.2239
- Xiang J, Wang K, Tang N. PCK1 dysregulation in cancer: metabolic reprogramming, oncogenic activation, and therapeutic opportunities. *Genes Dis.* 2023;10(1):101-112. doi:10.1016/j.gendis.2022.02.010

SUPPORTING INFORMATION

Additional supporting information can be found online in the Supporting Information section at the end of this article.

How to cite this article: Yao Y, Wang D, Zhang Y, et al. Peroxisome proliferator-activated receptors signature reveal the head and neck squamous cell carcinoma energy metabolism phenotype and clinical outcome. *J Gene Med*. 2023;e3605. doi:10.1002/jgm.3605